nature geoscience

LETTERS

PUBLISHED ONLINE: 4 SEPTEMBER 2011 | DOI: 10.1038/NGEO1242

Significant increase in relief of the European Alps during mid-Pleistocene glaciations

Pierre G. Valla[1]*, David L. Shuster[2,3] and Peter A. van der Beek[1]

Some of Earth's greatest relief occurs where glacial processes act on mountain topography[1,2]. This dramatic landscape is thought to be an imprint of Pleistocene glaciations[3,4]. However, whether the net effect of glacial erosion on mountains is to increase[5–7] or decrease[8–10] relief remains disputed. It has been suggested that in the European Alps, the onset of widespread glaciation since the mid-Pleistocene climate transition[11] led to the growth of large, long-lived and strongly erosive alpine glaciers[12,13] that profoundly influenced topography[14]. Here we use ^{4}He/^{3}He thermochronometry[15] and thermal-kinematic models to show that the Rhône Valley in Switzerland deepened by about 1–1.5 km over the past one million years. Our results indicate that while the valley was incised and back-cut, high-altitude areas were preserved from erosion. We find an approximately two-fold increase in both local topographic relief and valley concavity, which occurred around the time of the mid-Pleistocene transition. Our results support the proposed link[12–14] between the onset of efficient glacial erosion in the European Alps and the transition to longer, colder glacial periods at the middle of the Pleistocene epoch.

Understanding how the topographic relief of alpine landscapes develops and what controls this evolution requires quantifying the relative efficiency of fluvial, glacial and hillslope processes. Recent studies have suggested that glacial erosion efficiently shapes mountain-belt topography through glacial valley carving and cirque retreat[1,5–7], leading to significant relief increase at the valley scale (~5–10 km) and isostatic mountain-peak uplift in response to late Cenozoic climate cooling[4,6]. However, others have proposed that, because glacial erosion is most efficient around the Equilibrium Line Altitude (ELA), it should act as a 'glacial buzz-saw' to limit mountain height and therefore reduce topographic relief[8–10] at the drainage-basin scale. Therefore, understanding how mountain topography develops in response to climatic forcing (that is, glacial/interglacial oscillations) requires detailed quantitative information on the spatial and temporal patterns of erosion over ~10^6-year timescales.

In this study, we combine apatite (U–Th–Sm)/He dating[16] with ^{4}He/^{3}He thermochronometry[15] to constrain the timing and rate of glacial incision of a major Alpine valley and thus evaluate relief development at the valley scale. The (U–Th–Sm)/He system in apatite (AHe) is sensitive to cooling below ~80 °C and records bedrock exhumation through the uppermost 2–4 km beneath the Earth's surface[16]. Apatite ^{4}He/^{3}He thermochronometry constrains the spatial distribution of ^{4}He within individual apatite crystals and therefore the cooling history of specific samples below the AHe closure temperature[15] (see Methods and Supplementary Information). The resulting cooling histories may be compared at different locations[7,17] to test exhumation scenarios predicted by models of evolving topography[7,18].

We focus on the upper Rhône valley (Switzerland), one of the major drainage systems of the European Alps (Fig. 1a). The upper Rhône catchment features >3 km of topographic relief and contains several of the highest peaks of the Alps, with elevations at and above 4,000 m. It has been extensively glaciated during Quaternary glaciations[19,20]. The present-day morphology of the upper Rhône valley is typical of glacially influenced landscapes with U-shaped cross-profiles of 2–4 km width (Fig. 1b,c), a stepped longitudinal profile and major glacial overdeepenings[20]. We studied bedrock samples from two elevation transects along the Rhône valley at Martigny-Sion (SIO profile) and Visp (VIS profile), on the southern flanks of the Aiguilles Rouges and Aar massifs, respectively (Fig. 1a). These are two of the 'external crystalline massifs[21]' of the Alps; uplifted blocks of European crystalline basement characterized by high topography and relief, as well as a clear glacial imprint on landscape morphology. Previous studies have identified exhumation pulses within the external crystalline massifs during the late Neogene[22,23]. However, the exhumation and relief history throughout the Pliocene–Pleistocene remains incompletely resolved[22,23].

New AHe ages collected along the SIO and VIS profiles range from ~4 to 8 Myr and from ~1 to 5 Myr, respectively (see Supplementary Information); ages are positively correlated with elevation in both profiles (Fig. 1b,c). Apparent exhumation rates derived from age–elevation relationships are ~0.6 km Myr^{-1} (SIO profile) and ~0.9 km Myr^{-1} (VIS profile) during the time intervals spanned by the data. The AHe age–elevation relationships alone, however, do not tightly constrain the most recent exhumation and relief history of the area, as the inferred apparent exhumation rates integrate both exhumation and potential effects of topographic changes[18].

^{4}He/^{3}He thermochronometry of a subset of samples from both profiles (see Supplementary Information) constrains each sample's cooling history below ~80 °C and adds complementary information to decipher spatiotemporal variations in recent exhumation[7,15,17]. For instance, sample SIO-04 records a much more diffusive ^{4}He-distribution pattern than samples SIO-06 and -07 (Fig. 2). This requires that the valley-bottom sample (SIO-04) recently experienced more rapid cooling than the two samples (SIO-06 and -07) at higher elevations[15]. We use a numerical model[24] to constrain cooling paths from the observed AHe and ^{4}He/^{3}He data. For each sample, the inverse model randomly generates time–temperature histories, from which both an AHe age and ^{4}He distribution are predicted using a radiation-damage and annealing model to quantify He-diffusion kinetics in apatite (ref. 25 and references therein), and subsequently compared to the observed data (see Methods and Supplementary Information). This approach

[1]Institut des Sciences de la Terre, Université Joseph Fourier, CNRS, BP 53, F-38041 Grenoble, France, [2]Berkeley Geochronology Center, 2455 Ridge Road, Berkeley, California 94709, USA, [3]Department of Earth and Planetary Science, University of California, Berkeley, California 94720, USA.
*e-mail: pierre.valla@ujf-grenoble.fr.

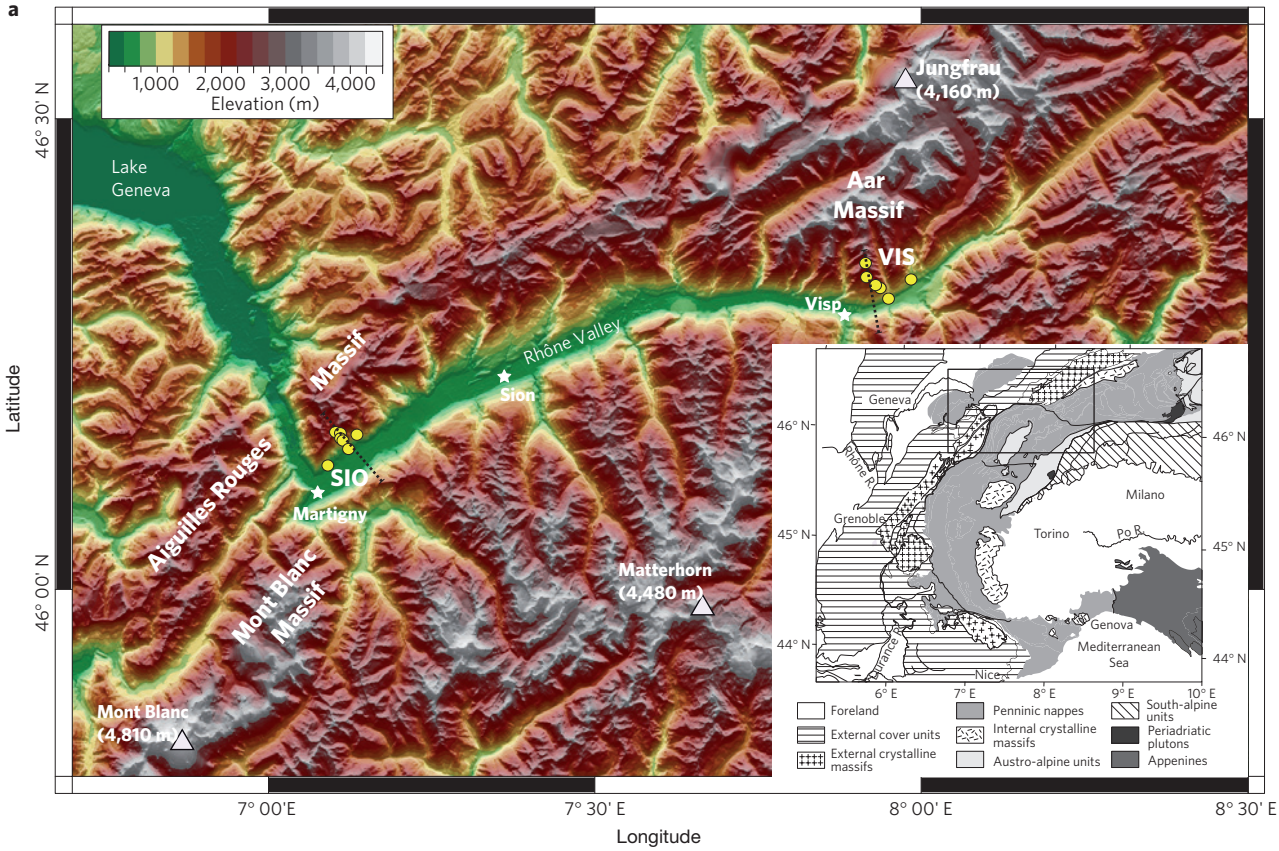

Figure 1 | Topography, sample locations and AHe age–elevation relationships. a, Relief map of the studied area. Yellow dots represent sampling sites. Inset shows location of the study area within the European Alps and major litho-tectonic units[21]. **b**,**c**, Martigny-Sion (SIO) and Visp (VIS) AHe age–elevation profiles. Red diamonds are mean AHe ages, bars show ±1 s.d., circles show single-crystal ages (filled: conventional AHe ages; open: ages derived from $^4He/^3He$ measurements). Dashed straight line is weighted linear regression; envelopes show 95% confidence limits on the age–elevation relationship; *r*: Pearson correlation coefficient; AER: apparent exhumation rate calculated from the weighted linear regression (±1 s.d.). Insets show sample locations along topographic cross-sections (dashed lines in Fig. 1a).

allows us to explore a wide range of cooling histories using a misfit-based evaluation of acceptable scenarios[7,24].

All SIO samples indicate rapid cooling from >6–7 Myr until around 5 Myr ago (Fig. 2 and Supplementary Fig. S2). However, cooling histories clearly differ since that time. The high-elevation sample SIO-06 (Fig. 2b) requires <10 °C cooling since 5 Myr ago and the mid-profile sample SIO-07 (Fig. 2d) permits only limited cooling (<25 °C) over the past 5 Myr. In contrast, the valley-floor sample SIO-04 (Fig. 2f) requires 4–5 Myr of residence within the AHe partial retention zone[16] (that is, 60–80 °C) before rapid cooling to surface temperatures initiating ~1 Myr ago. VIS samples also record rapid cooling ~6–4 Myr ago (Fig. 3 and Supplementary Figs S1, S2), although this initial cooling phase is less well resolved than for SIO samples because of younger AHe ages. However, the spatial pattern of cooling trends is similar: whereas the high-elevation sample VIS-03 (Fig. 3a) had cooled to surface temperatures by ~4 Myr ago, the lower-elevation samples VIS-04, -06 and -07 (Fig. 3b–d) all require significant cooling

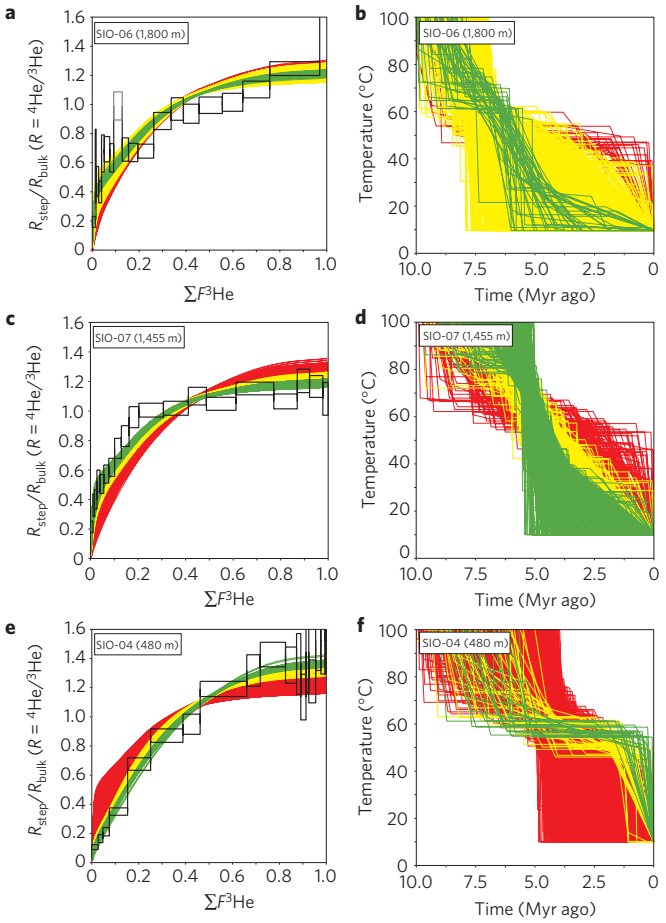

Figure 2 | $^4He/^3He$ thermochronometry of SIO samples. Observed $^4He/^3He$ ratio evolution diagrams and model cooling paths for **a**,**b**, SIO-06, **c**,**d**, SIO-07 and **e**,**f**, SIO-04. The measured $^4He/^3He$ ratios of each degassing step (R_{step}) are normalized to the bulk ratio (R_{bulk}) and plotted versus the cumulative ^3He release fraction ($\sum F^3He$). Boxes indicate ±1 s.d. (vertical) and integration steps (horizontal). Coloured lines show the predicted $^4He/^3He$ ratio evolution diagrams (**a**,**c**,**e**) for arbitrary cooling paths (**b**,**d**,**f**). Each coloured path predicts the observed AHe age of the sample to within ±1 s.d.; red and yellow cooling paths are excluded by the $^4He/^3He$ data, whereas green cooling paths are permitted (see Methods for details, and Supplementary Fig. S2 for supplementary sample SIO-02). All cooling paths initiated off scale at 150 °C; cooling paths that failed to predict the observed AHe age are not shown.

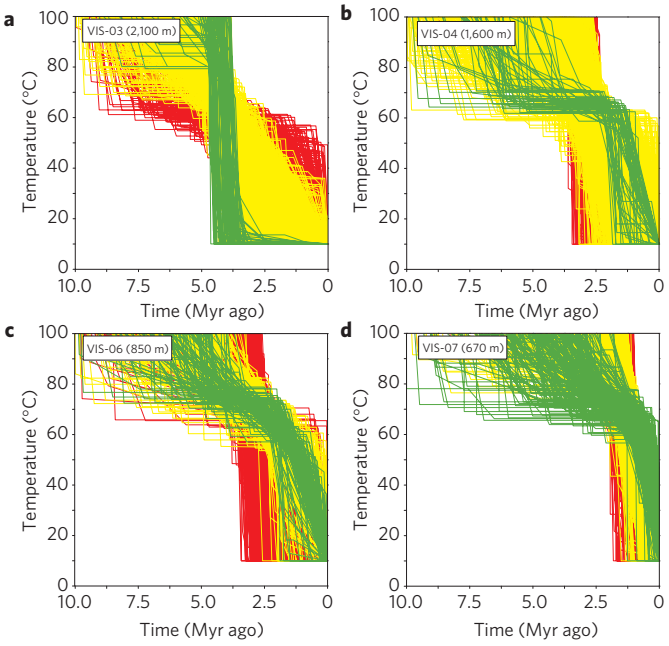

Figure 3 | Modelled cooling paths for VIS samples. Plots show cooling paths for samples **a**, VIS-03, **b**, VIS-04, **c**, VIS-06 and **d**, VIS-07. Colour coding is as in Fig. 2 (see Supplementary Fig. S1 for $^4He/^3He$ ratio evolution diagrams of these samples and Supplementary Fig. S2 for supplementary sample VIS-05). All cooling paths initiated off scale at 150 °C; cooling paths that failed to predict the observed AHe age are not shown.

in the past ~1 Myr from successively higher temperatures with decreasing sample elevation.

Thus, our analysis of AHe and $^4He/^3He$ data clearly indicates that both transects within the Rhône valley experienced a similar 3-step exhumation history during the late Miocene to Pleistocene: (1) a rapid phase of exhumation between 6–7 and ~4–5 Myr ago recorded by summit samples, followed by (2) a quiescent phase until ~1 Myr ago when (3) low-elevation samples record a recent episode of rapid cooling. The thermal histories constrained by the data incorporate sample-specific effects of radiation damage on He diffusion[24,25] (see Methods), yet both sites are in remarkable agreement with one another. We therefore conclude that the absolute AHe age difference between the two valley-bottom samples reflects the influence of different U and Th concentrations[25] together with mid-Pleistocene cooling from slightly different depths of partial ^4He retention. This exhumation history of the Rhône valley corroborates a late Miocene phase of exhumation in the external crystalline massifs of the Alps inferred from modelling thermochronological age–elevation profiles[22,23]. However, no unequivocal evidence for recent relief development was inferred from those previous studies. Our AHe and $^4He/^3He$ results clearly reveal substantial local exhumation beginning ~1 Myr ago within the Rhône valley in both transect locations, and minimal exhumation since ~5 Myr ago for high-elevation samples, implying a significant increase in local relief through valley incision.

To further quantify $^4He/^3He$-derived cooling paths in terms of background exhumation and potential relief changes, we use the thermal-kinematic model Pecube[18,26] (see Methods). Tested scenarios include three phases of exhumation over the past 10 Myr, as indicated by our $^4He/^3He$ results (Figs 2, 3) and previous modelling studies in neighbouring areas[22,23]. We focus on the late-stage exhumation and therefore test three different idealized exhumation scenarios to quantitatively compare modelled cooling paths with the $^4He/^3He$ data for summit and valley-floor samples: (1) constant or (2) temporally varying exhumation under fixed topography, and (3) relief increase through valley incision since 1 Myr ago (Fig. 4, see Methods for details).

Models 1 and 2, which include fixed topography, cannot explain simultaneous rapid cooling of the valley-floor samples over the past ~1 Myr (VIS-07 and SIO-04, Fig. 4b,d) and constant near-surface temperature conditions for the high-elevation samples (VIS-03 and SIO-06, Fig. 4a,c). The contrast between summit and valley-floor samples clearly requires significant relief increase in both locations (Model 3). The combined AHe ages, $^4He/^3He$ data and Pecube modelling results therefore indicate that the depth of the Rhône valley has increased by ~1 (SIO profile) to 1.5 (VIS profile) km since ~1 Myr ago, whereas high-elevation parts of the landscape only record modest erosion. This resulted in a roughly two-fold increase in local topographic relief (Fig. 4e), which we attribute to glacial valley lowering. An alternative scenario involving glacial valley widening predicts only ~20 °C of recent cooling at maximum, and cannot explain the $^4He/^3He$ data (see Supplementary Information). Using the above estimates of palaeo-valley floor elevations (Fig. 4e),

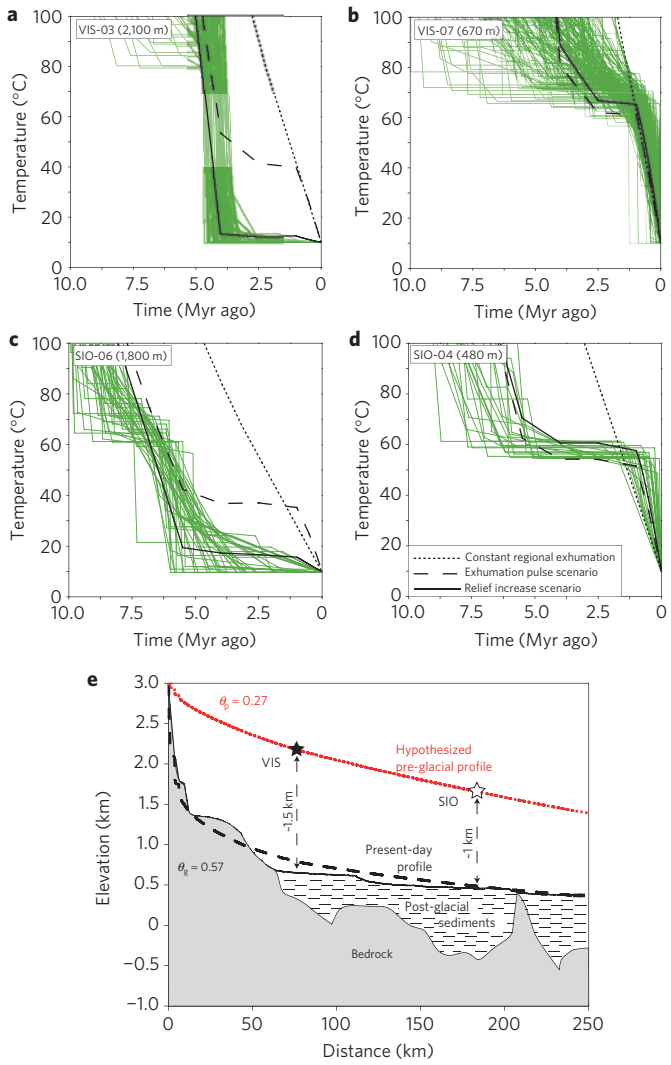

Figure 4 | Predicted cooling paths for different exhumation/relief scenarios and inferred Rhône valley evolution. a–d, Predicted cooling paths (black lines) using Pecube[26] compared to ^{4}He/^{3}He-derived best-fitting cooling paths (green lines) for VIS-03 (**a**), VIS-07 (**b**), SIO-06 (**c**) and SIO-04 (**d**). We test three idealized exhumation scenarios: (1) constant regional exhumation (dotted lines); (2) temporally varying exhumation under fixed topography (dashed lines); (3) relief increase through valley incision since ~1 Myr ago (solid black lines). See text for discussion. **e**, Present-day profile (black line) and pre-glacial reconstruction (red dashed line) of the Rhône valley. Bedrock glacial profile and post-glacial sediment fill are also shown[30]. Dashed lines correspond to best-fit smoothly concave profiles for present-day ($\theta_g \approx 0.57$) and pre-glacial reconstruction ($\theta_p \approx 0.27$). See Supplementary Information for details.

we propose a 'steady-state' fluvial profile reconstruction[20] of the pre-glacial Rhône valley (see Supplementary Information for details). The data and pre-glacial reconstruction indicate spatially variable and synchronous (that is, since ~1 Myr ago) incision of the Rhône valley. This resulted in both valley lowering and back-cutting, which led to a modern concavity index[20] twice that of the pre-glacial concavity estimate (~0.57 versus ~0.27, Fig. 4e).

Gradual cooling of Northern Hemisphere climate is thought to have initiated ~3.5 Myr ago[27]. This global climate transition, consistent with evidence for the existence of glaciers within the European Alps since the late Pliocene[19], clearly predates the km-scale valley incision since ~1 Myr ago inferred from our ^{4}He/^{3}He results. However, our data are consistent with cosmogenic-nuclide evidence for 1-km incision of the Aare valley, 50-100 km to the NE of our study area, dated at ~0.8–1.0 Myr ago[14]. Moreover, although these independent records of valley incision may lack comparable resolution in time, they are also consistent with the onset of major glacial sediment flux to the Po foreland basin, magneto-stratigraphically dated at ~0.87 Myr ago[12,13]. The onset of intense glaciations and rapid valley incision within the European Alps thus seems to correlate with the global mid-Pleistocene climatic transition from symmetric 41,000-year to strongly asymmetric 100,000-year glacial/interglacial oscillations[11]. This major climatic change may have enhanced glacial conditions by permitting larger, more erosive and longer-lived alpine glaciers to develop[12–14,28], which resulted in valley lowering through glacial incision while preserving high-elevation landscape elements. Moreover, the onset of asymmetric high-amplitude climate oscillations has enhanced erosion and topographic relief development by promoting transient landscapes and preventing fluvial processes from reaching steady-state conditions[20]. These results suggest that it was not solely the presence of alpine glaciers, but also the magnitude of climate oscillations[11–14] that promoted deep valley incision in the European Alps.

Apatite ^{4}He/^{3}He thermochronometry from the western European Alps reveals a ~100% increase in valley depth and significant valley back-cutting since ~1 Myr ago. In contradiction to the 'glacial buzzsaw' hypothesis[8,9], glacial valley incision clearly outpaced erosion at high-elevation regions of the landscape around or above both the present-day and the Last Glacial Maximum ELA. Thus, glaciations of the European Alps led to significant local (valley-scale) relief increase, which in turn should contribute to isostatic rock uplift in response to increased local erosion[29]. Unlike other alpine regions, where Pleistocene glacial incision may have been limited by decreasing areas of high-elevation catchments[7–10], the classic glaciated landscapes of the European Alps[3] seem to have been strongly affected by recent changes in the global climate system[11–14], which enhanced landscape disequilibrium and promoted valley incision and relief development through both glacial and fluvial processes[20]. The joint application of high-resolution thermochronometry and thermal-kinematic modelling holds great promise in quantifying the topographic response to climate changes and thereby testing theoretical model predictions for this response.

Methods

(U–Th–Sm)/He and ^{4}He/^{3}He thermochronometry. (U–Th–Sm)/He ages[16] were measured on single-crystal aliquots of apatite that were degassed by laser heating. ^{4}He abundances were measured using ^{3}He isotope dilution and quadrupole mass spectrometry, and U–Th–Sm concentrations were measured by isotope dilution using ICP-MS.

In ^{4}He/^{3}He thermochronometry[15], the spatial distribution of radiogenic ^{4}He is constrained by stepwise degassing of a sample containing synthetic, homogeneously distributed, proton-induced ^{3}He. Individual apatite crystals were heated in multiple steps under ultra-high vacuum to measure both the molar ^{3}He abundance and the ^{4}He/^{3}He ratio using calibrated pulse-counting sector-field mass spectrometry. The (U–Th–Sm)/He age was then calculated from U–Th–Sm concentrations and the total molar ^{4}He abundance summed from the incremental heating steps. Analytical measurements and uncertainties are given in the Supplementary Tables S1–S4.

The single-crystal, (U–Th–Sm)/He and ^{4}He/^{3}He-derived ages are both used to calculate a mean age (unweighted standard arithmetic mean[16]) and associated standard deviation (s.d.). Apparent one-dimensional exhumation rates are derived from linear error-weighted age–elevation regression (elevation being taken as the independent variable), for which reduced chi-squared values were close to one (1.1 and 1.6 for the VIS and SIO profiles, respectively), indicating that the regression is meaningful (as also shown by Pearson's coefficients in Fig. 1b,c).

Thermal modelling—inversion method. We use a recently developed numerical model[24] to predict an AHe age and the evolution of the ^{4}He/^{3}He ratio during a step-degassing analysis[15]. The model generates random time–temperature (t–T) paths and predicts an evolving spatial distribution of ^{4}He along each cooling path, assuming uniform spatial distribution of U–Th and an effective spherical diffusion geometry with surface/volume ratio equivalent to the analysed crystal,

and assuming the radiation damage and annealing model (RDAAM; ref. 25) quantifies the ^{4}He diffusion kinetics of each apatite sample. RDAAM relies on both U–Th content and the cooling history to fully model the time evolution of radiation damage within an apatite and its influence on He-diffusion kinetics[25]. To fully explore possible changes in He diffusivity through time, all cooling paths began at 150 °C, well above the accumulation of radiation damage effects[24,25]. For each randomly generated cooling history, the model first calculates a (U–Th)/He age that is compared to the measured age (Sm contribution to the AHe age is not incorporated into the model as it is insignificant compared with U–Th contributions). If the predicted age is within ±1 s.d. of the mean observed age (Supplementary Tables S2, S3), a model ^{4}He/^{3}He ratio evolution is calculated and compared to observed ratios to compute misfit statistics[24]; otherwise the model generates a new t–T path. Note that each coloured t–T path in Figs 2, 3 and Supplementary Figs S1, S2 predicts an AHe age that fits the observed age within ±1 s.d.; the colours indicate the degree of fit to the ^{4}He/^{3}He ratio evolution, as explained in the Supplementary Information.

3D Thermal-kinematic modelling—Pecube. Pecube is a 3D finite-element code[26] that solves the heat-transfer equation to predict thermal histories from input exhumation/relief scenarios[18]. The model parameters include crustal thickness (40 km; ref. 23), mean temperature at the surface (10 °C; based on present-day estimates) and the base of the domain (600 °C at 40 km depth[23]), and thermal diffusivity (25 km^2 Myr^{-1}; refs 22,23,26). A full inversion approach for exhumation and relief scenarios[18,22,23] is outside the scope of this study; our main objective is rather to illustrate what idealized exhumation scenarios are consistent with the ^{4}He/^{3}He-derived cooling paths, especially for the late-stage exhumation history since ~1 Myr ago. Therefore, we tested three idealized exhumation scenarios to quantify rock uplift and potential relief changes from ^{4}He/^{3}He-derived cooling paths. The simplest end-member scenario (Model 1) predicts cooling paths for a constant regional exhumation rate of 0.9 (VIS) or 0.6 (SIO) km Myr^{-1}, based on the AHe age–elevation relationships, and fixed relief over the past 10 Myr. The exhumation-pulse scenario (Model 2) shows the effect of a time-variable but spatially uniform exhumation rate with fixed present-day relief. The exhumation rate is 1.5 km Myr^{-1} for VIS (0.75 km Myr^{-1} for SIO) from 10 Myr to 4 Myr ago (5.5 Myr ago for SIO), based on the t–T paths of samples VIS-03 and SIO-06 and in agreement with exhumation histories reported for neighbouring areas[22,23]; 0.001 km Myr^{-1} until 1 Myr ago (to simulate a quiescent phase evidenced in nearly all SIO and VIS samples); and 1 km Myr^{-1} since 1 Myr ago (based on cooling paths of samples VIS-07 and SIO-04). The relief-increase scenario (Model 3) models the same transition in exhumation rate for VIS (from 1.5 to 0.001 km Myr^{-1} at 4 Myr ago) and SIO (from 0.75 to 0.001 km Myr^{-1} at 5.5 Myr ago); however the background exhumation rate is held at 0.001 km Myr^{-1} until present while imposing 1.0 (SIO) to 1.5 (VIS) km of valley incision starting 1 Myr ago (that is, palaeo-valley floor elevations at ~2,200 m and ~1,700 m for VIS and SIO, respectively, Fig. 4e).

Received 23 July 2010; accepted 1 August 2011; published online 4 September 2011

References

1. Brocklehurst, S. H. & Whipple, K. X. Response of glacial landscapes to spatial variations in rock uplift rate. *J. Geophys. Res.* **112,** F02035 (2007).
2. Meigs, A. & Sauber, J. Southern Alaska as an example of the long-term consequences of mountain building under the influence of glaciers. *Quat. Sci. Rev.* **19,** 1543–1562 (2000).
3. Penck, A. Glacial features in the surface of the Alps. *J. Geol.* **13,** 1–19 (1905).
4. Molnar, P. & England, P. Late Cenozoic uplift of mountain ranges and global climate change: Chicken or egg? *Nature* **346,** 29–34 (1990).
5. Montgomery, D. R. Valley formation by fluvial and glacial erosion. *Geology* **30,** 1047–1050 (2002).
6. Small, E. E. & Anderson, R. S. Geomorphically driven late Cenozoic rock uplift in the Sierra Nevada, California. *Science* **270,** 277–280 (1995).
7. Shuster, D. L., Cuffey, K. M., Sanders, J. W. & Balco, G. Thermochronometry reveals headward propagation of erosion in an alpine landscape. *Science* **332,** 84–88 (2011).
8. Brozovic, N., Burbank, D. & Meigs, A. Climatic limits on landscape development in the northwestern Himalaya. *Science* **276,** 571–574 (1997).
9. Egholm, D. L., Nielsen, S. B., Pedersen, V. K. & Lesemann, J-E. Glacial effects limiting mountain height. *Nature* **460,** 884–887 (2009).
10. Whipple, K. X., Kirby, E. & Brocklehurst, S. H. Geomorphic limits to climate induced increases in topographic relief. *Nature* **401,** 39–43 (1999).
11. Lisiecki, L. E. Links between eccentricity forcing and the 100,000-year glacial cycle. *Nature Geosci.* **3,** 349–352 (2010).
12. Muttoni, G. *et al.* Onset of major Pleistocene glaciations in the Alps. *Geology* **31,** 989–992 (2003).
13. Garzanti, E., Vezzoli, G. & Andò, S. Paleogeographic and paleodrainage changes during Pleistocene glaciations (Po Plain, Northern Italy). *Earth Sci. Rev.* **105,** 25–48 (2011).
14. Haeuselmann, P., Granger, D. E., Jeannin, P-Y. & Lauritzen, S-E. Abrupt glacial valley incision at 0.8 Ma dated from cave deposits in Switzerland. *Geology* **35,** 143–146 (2007).
15. Shuster, D. L. & Farley, K. A. ^{4}He/^{3}He thermochronometry. *Earth Planet. Sci. Lett.* **217,** 1–17 (2004).
16. Farley, K. A. (U–Th)/He dating: techniques, calibrations, and applications. in *Noble Gases in Geochemistry and Cosmochemistry* (eds Porcelli, D., Ballentine, C. J. & Wieler, R.) 819–844 (Reviews in Mineralogy and Geochemistry, Vol. 47, 2002).
17. Shuster, D. L., Ehlers, T. A., Rusmore, M. E. & Farley, K. A. Rapid glacial erosion at 1.8 Ma revealed by ^{4}He/^{3}He thermochronometry. *Science* **310,** 1668–1670 (2005).
18. Valla, P. G., Herman, F., van der Beek, P. A. & Braun, J. Inversion of thermochronological age–elevation profiles to extract independent estimates of denudation and relief history—I: Theory and conceptual model. *Earth Planet. Sci. Lett.* **295,** 511–522 (2010).
19. Schlüchter, C. The Quaternary glaciations of Switzerland, with special reference to the Northern alpine foreland. *Quat. Sci. Rev.* **5,** 413–419 (1986).
20. Norton, K. P., Abbühl, L. M. & Schlunegger, F. Glacial conditioning as an erosional driving force in the Central Alps. *Geology* **38,** 655–658 (2010).
21. Schmid, S. M., Fügenschuh, B., Kissling, E. & Schuster, R. Tectonic map and overall architecture of the Alpine orogen. *Ecl. Geol. Helv.* **97,** 93–117 (2004).
22. Glotzbach, C., van der Beek, P. A. & Spiegel, C. Episodic exhumation and relief growth in the Mont Blanc massif, Western Alps from numerical modelling of thermochronology data. *Earth Planet. Sci. Lett.* **304,** 417–430 (2011).
23. van der Beek, P. A. *et al.* Inversion of thermochronological age–elevation profiles to extract independent estimates of denudation and relief history—II: Application to the French Western Alps. *Earth Planet. Sci. Lett.* **296,** 9–22 (2010).
24. Schildgen, T. F., Balco, G. & Shuster, D. L. Canyon incision and knickpoint propagation recorded by apatite ^{4}He/^{3}He thermochronometry. *Earth Planet. Sci. Lett.* **293,** 377–387 (2010).
25. Flowers, R. M., Ketcham, R. A., Shuster, D. L. & Farley, K. A. Apatite (U–Th)/He thermochronometry using a radiation damage accumulation and annealing model. *Geochim. Cosmochim. Acta* **73,** 2347–2365 (2009).
26. Braun, J. Pecube: A new finite-element code to solve the 3D heat transport equation including the effects of a time-varying, finite amplitude surface topography. *Comp. Geosci.* **29,** 787–794 (2003).
27. Mudelsee, M. & Raymo, M. E. Slow dynamics of the Northern Hemisphere glaciation. *Paleoceanography* **20,** PA4022 (2005).
28. Berger, A. L. *et al.* Quaternary tectonic response to intensified glacial erosion in an orogenic wedge. *Nature Geosci.* **1,** 793–799 (2008).
29. Champagnac, J-D., Molnar, P., Anderson, R. S., Sue, S. & Delacou, B. Quaternary erosion-induced isostatic rebound in the western Alps. *Geology* **35,** 195–197 (2007).
30. Hinderer, M. Late Quaternary denudation of the Alps; valley and lake fillings and modern river loads. *Geodin. Acta* **14,** 231–263 (2001).

Acknowledgements

We thank J-D. Champagnac for field assistance, F. Cœur, B. Lum and F. Senebier for help during sample preparation. The staff of the Caltech Noble Gas Laboratory is acknowledged for conducting (U–Th–Sm)/He analyses. We thank G. Balco for development of the ^{4}He/^{3}He thermochronometry search algorithm, F. Chirouze and R. Delunel for fruitful discussions. M. Brandon and S. Brocklehurst provided constructive reviews. Financial support for this work was provided by the French Agence Nationale de la Recherche (ANR-08-BLAN-0303-01 grant to P.A.vd.B.), European Science Foundation Topo-Europe Eurocores programme, France-Berkeley Fund, US National Science Foundation (EAR-0720225 grant to D.L.S.) and the Ann and Gordon Getty Foundation.

Author contributions

P.G.V. conducted fieldwork, processed samples and performed numerical modelling; P.G.V. and D.L.S. conducted ^{4}He/^{3}He analyses; all authors contributed equally to the design of the study and writing of the paper.

Additional information

The authors declare no competing financial interests. Supplementary information accompanies this paper on www.nature.com/naturegeoscience. Reprints and permissions information is available online at http://www.nature.com/reprints. Correspondence and requests for materials should be addressed to P.G.V.